J|A|C|S COMMUNICATIONS

Published on Web 08/10/2009

Double-Shelled Nanocapsules of V_2O_5-Based Composites as High-Performance Anode and Cathode Materials for Li Ion Batteries

Jun Liu,[†] Hui Xia,[‡] Dongfeng Xue,*[,†] and Li Lu[‡]

State Key Laboratory of Fine Chemicals, Department of Materials Science and Chemical Engineering, School of Chemical Engineering, Dalian University of Technology, 158 Zhongshan Road, Dalian 116012, P. R. China, and Department of Mechanical Engineering, National University of Singapore, 9 Engineering Drive 1, Singapore 117576, Singapore

Received July 6, 2009; E-mail: dfxue@chem.dlut.edu.cn

Safe, low-cost, high-energy-density, and long-lasting rechargeable Li ion batteries are urgently needed in today's information-rich, mobile, and energy-conscious society.[1−3] For Li ion battery cathodes, vanadium pentoxide (V_2O_5) has been attracting much attention, as it offers the essential advantages of low cost, abundant sources, and better safety relative to commercial cathodes such as $LiCoO_2$ and $LiNiO_2$.[1c] V_2O_5 can serve as the anode in Li ion battery design, while it may be used as the cathode material in rechargeable Li ion batteries.[1,4] In this study, we have designed a new double-electrode nanomaterial composed of a V_2O_5 matrix containing a low weight ratio of SnO_2 nanocrystals (10 or 15%). In this nanostructured composite electrode material, the SnO_2 nanocrystals are homogenously distributed in a double-shelled V_2O_5 hollow nanocapsule. This nanocomposite is found to show high performance as both an anode and cathode material in Li ion batteries.

The $V_2O_5-SnO_2$ double-shelled nanocapsules were synthesized by a solvothermal treatment and final heat treatment in air (see the Supporting Information). The X-ray diffraction (XRD) pattern of the nanocomposites (Figure 1) showed that all of the Bragg peaks are consistent with those of a tetragonal SnO_2 phase (space group $P4_2/mnm$, $a = 4.7382$ Å, $c = 3.1871$ Å; JCPDS no. 41-1445) and an orthorhombic V_2O_5 phase (space group $Pmmn$, $a = 11.516$ Å, $b = 3.5656$ Å, $c = 4.3727$ Å; JCPDS no. 41-1426). Inductively coupled plasma (ICP) emission spectrometry was used to confirm the precise chemical composition of these nanocomposites, and they were found to contain 90 wt % V_2O_5 and 10 wt % SnO_2. The energy-dispersive X-ray spectroscopy (EDS) pattern (Figure S1b in the Supporting Information) showed that each nanocapsule is composed of Sn, V, and O, which is consistent with the XRD measurements and ICP analyses. The EDS analysis showed that the atomic ratio between Sn and V in these nanocomposites is close to their initial precursor molar ratio in the reaction mixture.

An overview scanning electron microscopic (SEM) image of the $V_2O_5-SnO_2$ nanocapsules (Figure 2a) indicates that these nanocomposites can be produced on large scale with an average diameter of 550 nm and without aggregation. The inset of Figure 2a shows a schematic structure of one of these double-shelled nanocomposite capsules. The red spheres represent SnO_2 nanocrystals, and the green double shells represent the V_2O_5 matrix. The microstructure and components of these nanocapsules were further studied by means of transmission electron microscopy (TEM) and selected-area electron diffraction (SAED). Figure 2b shows a low-magnification TEM image displaying double-shelled $V_2O_5-SnO_2$ nanocapsules consisting of nanocrystals. A typical double-shelled nanocapsule is shown in Figure 2c, which clearly confirms that these hollow

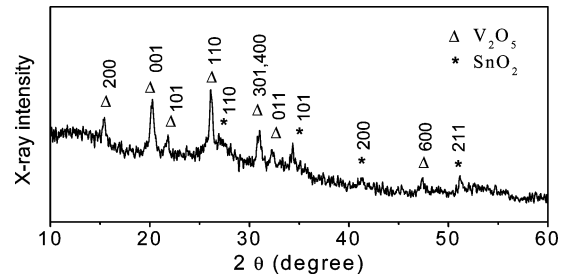

Figure 1. XRD pattern of V_2O_5-based nanocomposites as double-shelled hollow nanocapsules.

nanocapsules have two thin shells. The diameter of the inner hollow nanocapsules is ∼430 nm, and the inner cavity size is ∼250 nm. From the high-magnification TEM image shown in Figure 2d, the thickness of the inner and outer walls can be determined to be ∼90 nm. To investigate the distribution mode of SnO_2 in the shell, high-resolution TEM (HRTEM) characterization was carried out. The micrographs in Figure 2e−g are HRTEM images taken from the wall edge of the nanocapsules shown in Figure 2d at different locations. Figure 2e shows a HRTEM image of a single nanocrystal that reveals the (310) lattice planes of V_2O_5. Micrographs 2f and 2g reveal the (110) and (101) lattice planes of SnO_2, respectively. These HRTEM images confirm that the SnO_2 nanocrystals are homogenously distributed in the V_2O_5 matrix (double shells). The polycrystalline nature of these nanocapsules was also confirmed by the SAED measurements (Figure 2h). The formation mechanism of the current double-shelled hollow nanocapsules is a combination of two types of Ostwald ripening processes (both inward and outward ripening cases), as discussed in detail in the Supporting Information.

The anode performance of the V_2O_5-based nanocomposites is shown in Figure 3. Figure 3a shows the first two charge/discharge curves of a $Li/V_2O_5-SnO_2$ cell in the voltage window of 0.01−3 V at a current density of 250 mA g^{-1}. The first discharge and charge capacities are 1776 and 947 mA h g^{-1}, respectively. The large reversible capacity of 947 mA h g^{-1} is the first of this size reported for V_2O_5-based electrode materials. Multiple voltage plateaus due to different redox reactions associated with Li insertion/extraction can be observed in the first charge and discharge curves. These redox reactions can be better illustrated using cyclic voltammetry (CV) curves, as shown in Figure 3b. The four reduction peaks located at 3.14, 2.51, 2.30, and 1.88 V for the first discharge can be assigned to successive phase transformations upon lithium ion insertion via V_2O_5, giving ϵ-$Li_xV_2O_5$, δ-$Li_xV_2O_5$, γ-$Li_xV_2O_5$, and ω-$Li_xV_2O_5$, respectively. Although SnO_2 theoretically possesses a very high capacity of 1494 mA h g^{-1} at 8.4Li insertion,[1a] the majority of the capacity for this $V_2O_5-SnO_2$ composite is from

[†] Dalian University of Technology.
[‡] National University of Singapore.

10.1021/ja9053256 CCC: $40.75 © 2009 American Chemical Society

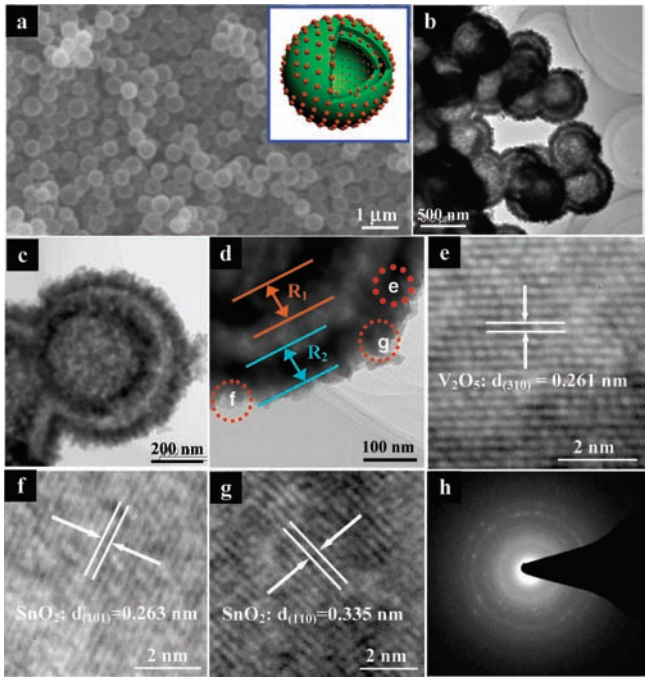

Figure 2. (a) SEM image of $V_2O_5-SnO_2$ double-shelled nanocapsules. The inset shows a schematic structure of a double-shelled nanocapsule. The red spheres represent SnO_2 nanocrystals, and the green double shells represent the V_2O_5 matrix. (b) Low-magnification TEM image. (c, d) High-magnification TEM images showing that the porous shells consist of a great deal of nanocrystals and have thicknesses of $R_1 \approx R_2 = 90$ nm. (e−g) HRTEM images revealing lattice planes of the V_2O_5 matrix and SnO_2 nanocrystals. (h) SAED pattern taken from individual nanocapsules, which shows that these nanocapsules are polycrystalline.

V_2O_5 because only 10 wt % of the composite is SnO_2. If it is assumed that V_2O_5 can be reduced to metallic V when this composite is discharged to 0 V versus Li/Li^+, the theoretical capacity for the Li insertion reaction is 1471 mA h g^{-1}, which can explain the high reversible capacity of this nanocomposite as an anode material. The first discharge capacity is even larger than the theoretical capacity of V_2O_5, which is plausibly attributed to the formation of a surface−electrolyte interphase film via electrolyte decomposition.[5] Charge/discharge curves at different current densities (Figure 3c) show that these nanocomposites exhibit a good rate capability as the anode material. Even at a high current density of 2500 mA g^{-1}, this material can still deliver a reversible capacity of 505 mA h g^{-1}. Figure 3d shows the cycle performance of this anode material at a current density of 250 mA g^{-1} for 50 cycles. After 50 cycles, the nanocomposites can still deliver a reversible capacity of 673 mA h g^{-1}, which is 70% of its initial capacity. For the nanocomposite as a cathode material, the small quantity of SnO_2 in the nanocomposite does not degrade its cathode performance. This nanocomposite delivers a reversible capacity of 174 mA h g^{-1} (82% of its initial capacity) after 50 cycles at a current density of 100 mA g^{-1} and exhibits good rate capability (Figure S5).

Double-shelled nanocapsules provide convenient access to Li ion ingress/egress and have more locations (such as a hollow interior and defects in the two walls of hollow capsules) for Li ion storage,[6] which are helpful in improving the battery capacity. In addition, Sn nanoparticles (generated during the reduction process of SnO_2 when the nanocomposite is used as an anode) are embedded in the V_2O_5 matrix, which forms an ultrafine metal−oxide electrode. Electrode materials made by this process may have some outstanding advantages, such as a reduced first-cycle irreversibility, good

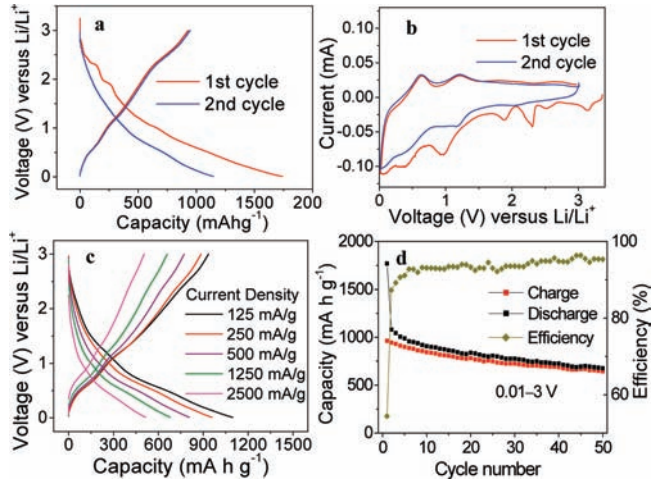

Figure 3. Anode performance of the as-prepared V_2O_5-based nanocomposites with 10 wt % SnO_2. (a) First two cycles of charge/discharge curves at a current density of 250 mA g^{-1}. (b) First two cycles of CV curves at a scan rate of 0.1 mV s^{-1}. (c) Charge/discharge curves at different current densities. (d) Capacity (left) and efficiency (right) versus cycle number at a current density of 250 mA g^{-1}, showing the charge and discharge capacity.

tolerance for cyclic volume variations, and high electronic and ionic conductivity.[7]

In conclusion, we have developed a solution-based method for the large-scale synthesis of self-assembled $V_2O_5-SnO_2$ double-shelled nanocapsules. The current nanoarchitecture provides short Li ion pathways and high electronic and ionic conductivity, and the hollow architecture is able to accommodate large volume variations. As anode and cathode materials for Li ion batteries, the V_2O_5-based nanocomposites exhibit a very high reversible capacity, excellent cycling performance, and good rate capability. This synthesis method is highlighted by its simplicity and high-yield production of a well-defined capsule morphology with a uniform diameter, which has promising industrial merits. This template-free route can be extended to the fabrication of other oxide composites with unique hollow architectures.

Acknowledgment. D.X. thanks the NSFC (Grant 50872016) for financial support. L.L. and H.X. thank the National University of Singapore for support.

Supporting Information Available: Experimental details, TEM characterizations of intermediate products, and additional electrochemical characterizations of nanocomposites. This material is available free of charge via the Internet at http://pubs.acs.org.

References

(1) (a) Arico, A. S.; Bruce, P.; Scrosati, B.; Tarascon, J. M.; Schalkwijk, W. V. *Nat. Mater.* **2005**, *4*, 366. (b) Whittingham, M. S. *Chem. Rev.* **2004**, *104*, 4271. (c) Wang, Y.; Cao, G. Z. *Adv. Mater.* **2008**, *20*, 2251.
(2) (a) Xia, H.; Lu, L.; Meng, Y. S. *Appl. Phys. Lett.* **2008**, *92*, 011912. (b) Xia, H.; Lu, L.; Meng, Y. S. *J. Electrochem. Soc.* **2007**, *154*, A337.
(3) (a) Chen, H.; Armand, M.; Courty, M.; Jiang, M.; Grey, C. P.; Dolhem, F.; Tarascon, J. M.; Poizot, P. *J. Am. Chem. Soc.* **2009**, *131*, 8984. (b) Lee, K. T.; Kan, W. H.; Nazar, L. F. *J. Am. Chem. Soc.* **2009**, *131*, 6044.
(4) (a) Odani, A.; Pol, V. G.; Pol, S. V.; Koltypin, M.; Gedanken, A.; Aurbach, D. *Adv. Mater.* **2006**, *18*, 1431. (b) Prosini, P. P.; Xia, Y. Y.; Fujieda, T.; Vellone, R.; Shikano, M.; Sakai, T. *Electrochim. Acta* **2001**, *46*, 2623. (c) Cohen, Y. S.; Aurbach, D. *Electrochem. Commun.* **2004**, *6*, 536.
(5) Ein-Eli, Y. *Electrochem. Solid-State. Lett.* **1999**, *2*, 212.
(6) (a) Liu, J.; Xue, D. *Adv. Mater.* **2008**, *20*, 2622. (b) Yan, C.; Xue, D. *Adv. Mater.* **2008**, *20*, 1055. (c) Liu, J.; Liu, F.; Gao, K.; Wu, J.; Xue, D. *J. Mater. Chem.* [Online early access]. DOI: 10.1039/b900116f. Published Online: May 8, 2009. (d) Yan, C.; Xue, D. *Electrochem. Commun.* **2007**, *9*, 1247.
(7) Limthongkul, P.; Wang, H. F.; Chiang, Y. M. *Chem. Mater.* **2001**, *13*, 2397.

JA9053256